ResearchGate

See discussions, stats, and author profiles for this publication at: https://www.researchgate.net/publication/267929546

Effect of Auxiliary Chromophores on the Optical, Electrochemical, and Photovoltaic Properties of Carbazole-Based Dyes

ARTICLE *in* ASIAN JOURNAL OF ORGANIC CHEMISTRY · NOVEMBER 2014

Impact Factor: 3.32 · DOI: 10.1002/ajoc.201402235

CITATIONS
5

READS
38

4 AUTHORS, INCLUDING:

Justin Thomas K R
Indian Institute of Technology Roorkee
153 PUBLICATIONS **4,386** CITATIONS
SEE PROFILE

Chuan-Pei Lee
University of California, Berkeley
78 PUBLICATIONS **1,297** CITATIONS
SEE PROFILE

Available from: Chuan-Pei Lee
Retrieved on: 25 January 2016

ACES

DOI: 10.1002/ajoc.201402235

ASIAN JOURNAL OF ORGANIC CHEMISTRY
Full Paper

Dye-Sensitized Solar Cells

Effect of Auxiliary Chromophores on the Optical, Electrochemical, and Photovoltaic Properties of Carbazole-Based Dyes

A. Venkateswararao,[a] K. R. Justin Thomas,*[a] Chuan-Pei Lee,[b] and Kuo-Chuan Ho[b]

Abstract: Organic dyes containing 2-diphenylaminocarbazole donors and decorated with auxiliary chromophores at the diphenylamine moiety have been synthesized and characterized. The nature of the chromophores on diphenylamine unit alters the light-harvesting properties and HOMO/LUMO energies of the dyes. Butoxy substitution raises the HOMO and lowers the LUMO energies. But the incorporation of fluorenyl units fine-tunes the LUMO upwardly, which improves the thermodynamic driving force for electron injection into the conduction band of TiO_2 and hikes the incident photon-to-current conversion efficiency. Consequently, a dye with fluorene in the donor unit and thiophene in the π-conjugation pathway is the most efficient (5.76%) and has the highest photocurrent density (14.60 mA cm^{-2}) in the series. Electrochemical impedance analysis of the devices showed the importance of fluorene units in suppressing electron recombination.

Introduction

Organic materials suitable for application in light-emitting diodes, thin-film transistors, and photovoltaic devices have received immense attention in recent years.[1–3] Despite the dominance of inorganic/organometallic materials in electronic devices, because of their favorable electronic structure and superior performance, organic small molecules continue to enjoy research focus due to their versatile functional properties, which, in turn, can be fine-tuned by small structural alterations.[4] Dipolar compounds featuring suitable electronic-donors and acceptors have been widely demonstrated as efficient functional materials in electronic devices.[5] Particularly, organic dyes that display effective intramolecular charge separation have been found beneficial role as sensitizers in dye-sensitized solar cells (DSSCs).[4b–f]

Organic dyes can be divided into two broad categories, one containing triarylamine donors while the others have heterocyclic donors. Triarylamines as donors impart several benefits, such as red-shifted absorption with high molar extinction coefficients arising from the strong donor strength, and inhibition of aggregation by the trigonal geometry of the molecular materials.[6] In addition, the electronic properties and the structural diversity can be enhanced by the attachment of auxiliary chromophores to the triarylamine unit.[6b] Fine-tuning of the frontier molecular orbital (highest occupied molecular orbital (HOMO) and lowest unoccupied molecular orbital (LUMO)) energies are required to achieve efficient electron injection from the dye into the conduction band of TiO_2 and facile regeneration of the oxidized dyes by a redox couple.[7]

Besides donors, the linker that mediates the electronic interaction between the donor and acceptor has also been found to be crucial in determining the efficacy.[4b–f] Fused heterocyclic polyaromatics have been exemplified as efficient mediators for donor–acceptor interactions in organic dyes.[8,9] Structural attachments that affect the coplanarity of the conjugation pathway have been found to influence the absorption as well as associated properties. Since the nature of the auxiliary chromophores attached to the donor and linker drastically affect the electronic properties of the dyes, the choice of group is crucial. Electron-donating units normally bathochromically shift the absorption spectrum with a concomitant upward movement in the HOMO level.[4b–f] High-lying HOMO values reduce the thermodynamic driving force for the regeneration of the dye.[7] However, the presence of weak acceptors or π-delocalizing groups in the donor segment has been found to fine-tune the HOMO and LUMO energies favorably.[10]

Sun and co-workers reported that incorporation of a 2,4-dibutoxyphenyl unit on the periphery of triphenylamine donor decreases the electron recombination with the redox species in the electrolyte and leads to huge increase of the V_{OC}.[11] Frey and co-workers reported the use of alkoxy-substituted fluorene-based amine donors and achieved good efficiency in DSSCs.[8b,c] Promarak and co-workers found that the use of additional carbazole donors resulted in red-shifted absorption

[a] A. Venkateswararao, Dr. K. R. Justin Thomas
Organic Materials Laboratory
Department of Chemistry
Indian Institute of Technology Roorkee
Roorkee 247 667 (India)
E-mail: krjt8fcy@iitr.ac.in

[b] Dr. C.-P. Lee, Prof. K.-C. Ho
Department of Chemical Engineering
National Taiwan University
Taipei 10617 (Taiwan)

Supporting information for this article is available on the WWW under http://dx.doi.org/10.1002/ajoc.201402235.

© 2015 Wiley-VCH Verlag GmbH & Co. KGaA, Weinheim

and a hike in J_{SC}.[12] Sun et al. found that the use of alkoxy groups on triarylamine donors diminished the aggregation of dyes and reduced back electron transfer.[8a] Yang and co-workers observed a similar effect due to a 2,4-dibutoxyphenyl unit on phenothiazine-based organic dyes.[13] Jia and co-workers incorporated imidazole units on triphenylamine-based dyes and found that planar imidazoles facilitated the formation of aggregates on the TiO_2 surface and led to blue-shifted absorption, whereas nonplanar imidazoles improved the molar extinction coefficient and broadened the incident photon-to-current conversion efficiency (IPCE) spectra.[14] Zheng and co-workers synthesized pyridine-, thiophene-, and pyrazole-substituted triphenylamine dyes and found that the thiophene and pyrazole units red-shifted the absorption and helped to delocalize the positve charge upon photooxidation.[7d]

The dye-regeneration capacity of most of the dyes that contain electron-rich auxiliary chromophores or linkers is poor due to the reduced thermodynamic driving force for the dye-regeneration by the redox shuttle caused by the high-lying HOMO of the dye. We hypothesized that the use of weakly electron-donating fluorene in place of an alkoxy unit would help to circumvent this problem. Fluorene also offers methods to incorporate alkyl chains on the sp^3 carbon at the C9 position, which may increase the electron recombination resistance.[15] To test this proposal, we have designed four dyes (Figure 1) based on a 2,7-disubstituted carbazole linker that contain different *n*-butoxy or fluorene units on the donor. We found that the fluorene substitution is beneficially for realizing favorable HOMO and LUMO energy levels and enhanced light-harvesting properties.

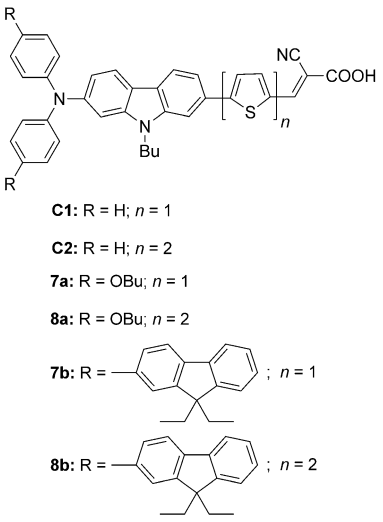

Figure 1. Structures of the dyes.

Results and Discussion

Synthesis and Characterization

The syntheses of the dyes were accomplished as shown in Scheme 1. The synthetic pathways for the dyes involved palladium-catalyzed protocols such as Buchwald–Hartwig C–N coupling,[16] Suzuki[17] and Stille[18] C–C coupling, and copper catalyzed C–O coupling[19] reactions. In the first step, the *n*-butoxy or fluorene functionalized diphenylamine (**2**) was prepared by either copper-catalyzed C–O coupling[19] with butanol, or palladium catalyzed C–C coupling[17] with 9,9-diethyl-9*H*-fluoren-2-ylboronic acid.[20] Further, the secondary amines **2** were converted into the triarylamines **4** by treatment with 2,7-dibromo-9-butyl-9*H*-carbazole (**3**) under the Buchwald–Hartwig C–N coupling conditions.[16] Then, the Stille coupling reaction[18] of **4** with the appropriate tin reagents derived from thiophene or bithiophene aldehydes followed by acidic hydrolysis generated the required aldehydes **5** and **6**. Finally, the target dyes **7** and **8** were synthesized by Knoevenagel condensation[21] of the aldehydes **5** and **6** with cyanoacetic acid in the presence of ammonium acetate. All the new compounds were thoroughly characterized by IR and NMR spectroscopy (^1H and ^{13}C) and mass spectrometry. The proposed structures are consistent with the spectral data. The dyes are generally dark red

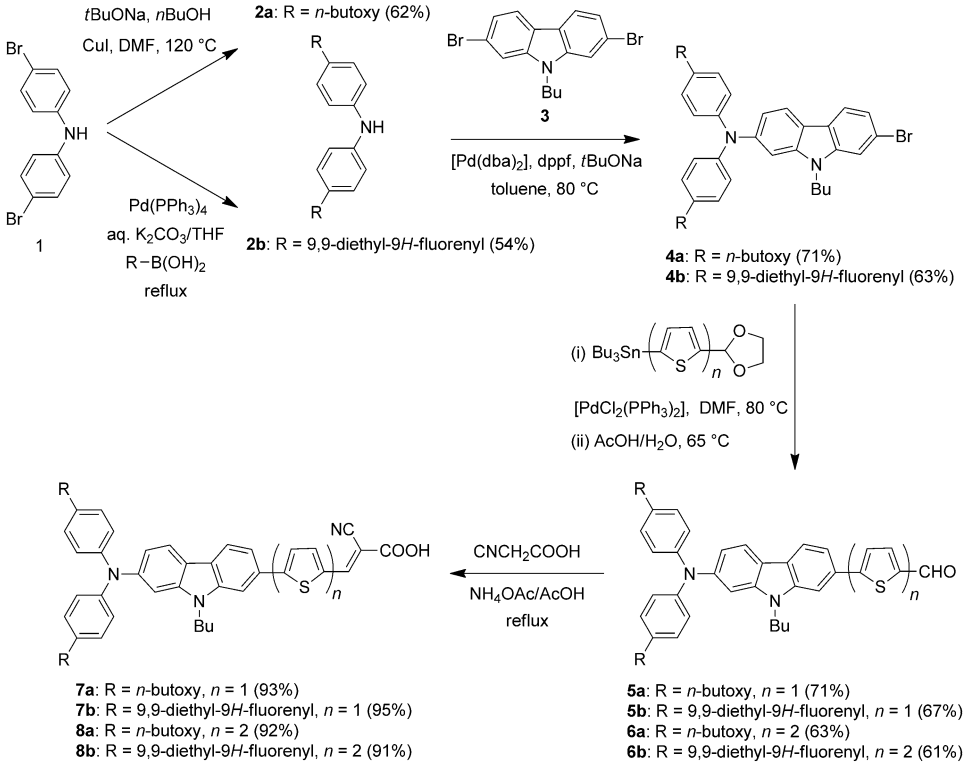

Scheme 1. Synthesis of the dyes.

© 2015 Wiley-VCH Verlag GmbH & Co. KGaA, Weinheim

in color and dissolve completely in common organic solvents such as dichloromethane (DCM), tetrahydrofuran (THF), dimethyl sulfoxide (DMSO), *N*,*N*-dimethylformamide (DMF), and so on.

Photophysical Properties

To quantify the light-absorbing capability of the dyes, optical spectra of the dyes and their precursors were measured in dichloromethane. Absorption spectra of the dyes are displayed in Figure 2 and the pertinent data compiled in Table 1. All the

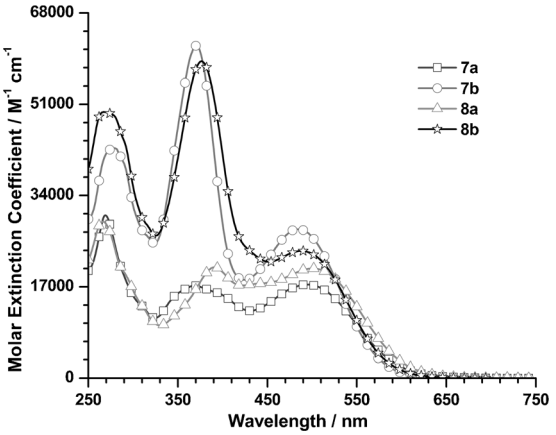

Figure 2. Absorption spectra of dyes **7** and **8** recorded in CH_2Cl_2.

dyes possess three well resolved bands at ca. 270, 370 and 490 nm. The shorter wavelength absorptions are attributed to π–π* transitions originating from the triarylamine, fluorene, carbazole, and thiophene segments. The increase in the intensity observed for the fluorene-containing dyes **7b** and **8b** shows the elongation in the conjugation due to fluorene attachment. The longest wavelength absorption is assigned to an intramolecular charge transfer (ICT) transition. This ICT transition is slightly red-shifted for the *n*-butoxy derivatives **7a** and **8a** compared with the fluorene derivatives **7b** and **8b**. However, the molar extinction coefficient of the fluorene derivatives is marginally higher than that of the *n*-butoxy analogues. These results indicate that the *n*-butoxy substitution increases the donor strength; however, due to the elongated π-conjugation rendered by the fluorene unit, the transition probability of the ICT absorption is increased. This suggests that the incorporation of an electron-rich conjugated aromatic/heteroaromatic segment is beneficial to increase the molar extinction coefficient of the ICT transition compared with simple electron-donating alkoxy or amino groups. It is also interesting to compare the absorption parameters with that of the parent dyes **C1** and **C2**, which contain unsubstituted diphenylamine donors.[22] The ICT band of the new dyes was apparently red-shifted compared with the parent dyes, which is attributable to the presence of peripheral *n*-butoxy or fluorene units. The red-shift is more pronounced for the *n*-butoxy substitution; however, this is at the expense of molar extinction coefficient. The molar extinction coefficients of the dyes are high compared with promising organometallic ruthenium dyes such as **N3** (13900 $M^{-1}cm^{-1}$) and **N719** (14000 $M^{-1}cm^{-1}$).[4g]

The solvatochromism of the dyes was examined by recording the absorption spectra of the dyes in different solvents to confirm the nature of the ICT band. An illustrative example of solvatochromism in the dyes is displayed in Figure 3a for the dye **7b**. In general, the ICT bands of all the dyes blue-shifts on increasing the polarity, which is indicative of negative solvatochromism. This is suggestive of a more polar ground state for the dyes which is preferentially stabilized by the polar solvents by effective solvation. The shorter wavelength absorptions attributed to the π–π* transitions did not change their position with solvent polarity. The unusual red-shifted absorption observed for the dyes in dichloromethane originates from the rapid stabilization of polarizable electrons during electronic excitation.[23] The more pronounced blue-shift observed for the DMF solution is ascribed to the basic nature of the medium, which shifts the acid-base equilibrium in this class of dyes to the deprotonated form.[24] In the deprotonated form, the donor-acceptor interaction is weakened, which results in a blue-shifted absorption.

Table 1. Optical and electrochemical data for the dyes measured in CH_2Cl_2.

Dye	λ_{abs} [nm] [$\varepsilon_{max}\times10^3$ $M^{-1}cm^{-1}$]	λ_{em} [nm]	Stokes shift [cm^{-1}][a]	E_{ox} [V][b]	HOMO [eV][c]	LUMO [eV][d]	E_{0-0} [eV][e]	E_{ox}* [V][f]
4a	356 (16.6), 270 (25.1)	449	5818	0.14 (65), 0.74	4.94	1.88	3.06	-2.15
4b	374 (80.8), 279 (51.4)	445	4266	0.32 (67), 0.83	5.12	2.08	3.04	-1.95
5a	431 (22.9), 313(18.1), 274 (25.9)	515	3784	0.14 (68), 0.72	4.94	2.62	2.32	-1.41
5b	424 (40.1), 370 (63.0), 280 (53.2)	574	6163	0.32 (65), 0.81	5.12	2.59	2.53	-1.44
6a	443 (28.3), 360 (18.0), 272 (29.2)	557	4620	0.12 (70), 0.66	4.92	2.66	2.26	-1.37
6b	425 (47.3), 373 (73.8), 279 (51.8)	503	3649	0.30 (67), 0.72	5.10	2.45	2.65	-1.58
C1	472 (29.3), 357 (18.0), 311 (16.8)	572	3704	0.38 (65), 0.86	5.18	2.85	2.33	-1.18
C2	489 (34.3), 375 (23.5), 311 (16.9), 264 (34.6)	579	3179	0.33 (52), 0.71	5.13	2.86	2.27	-1.17
7a	495 (17.4), 369 (17.2), 269 (30.3)	565	2503	0.13 (68), 0.71	4.93	3.10	1.85	-0.95
7b	485 (27.7), 371 (61.9), 279 (42.8)	570	3075	0.32 (61), 0.80	5.12	2.73	2.39	-1.30
8a	500 (20.5), 390 (20.6), 266 (29.2)	545	1651	0.12 (52), 0.65	4.92	3.12	1.83	-0.94
8b	488 (23.7), 376 (59.0), 267 (50.0)	575	3100	0.28 (58), 0.69	5.08	2.74	2.34	-1.29

[a] From $1/\lambda_{abs}$-$1/\lambda_{em}$. [b] Oxidation potentials are reported with reference to the ferrocene internal standard. [c] Deduced from the oxidation potential using the formula HOMO = 4.8 + E_{ox}. [d] Calculated using the formula LUMO = HOMO − E_{0-0}. [e] Calculated from the intersection of absorption and emission spectra. [f] Calculated from $E_{ox}^* = E_{ox} - E_{0-0}$.

© 2015 Wiley-VCH Verlag GmbH & Co. KGaA, Weinheim

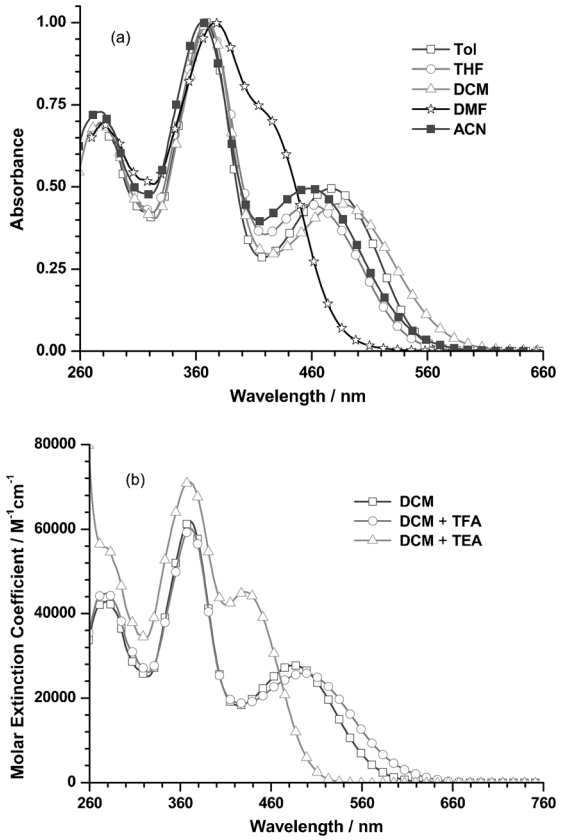

Figure 3. Absorption spectra of the dye **7b** recorded in (a) different solvents and (b) in the presence of TFA/TEA.

The existence of acid-base equilibrium for the dyes was confirmed by the influence of trifluoroacetic acid (TFA) and triethylamine (TEA) on the absorption spectra of the dyes (Figure 3b). The addition of TFA generally pushes the equilibrium towards the neutral form of the dye and results in a red-shifted absorption, while TEA deprotonates the dye and gives rise to the blue-shifted absorption.[25] As expected, the addition of TEA to the dichloromethane solution of the dyes shifts the absorption drastically to the shorter wavelength region, but TFA addition only caused a minor change, which suggests that the dyes are predominantly in the neutral form in dichloromethane solutions. Further the progressive red-shift observed on moving from the precursor bromides **4** < aldehydes **5** and **6** to the dyes **7** and **8** confirmed the assignment of ICT character to the lowest energy absorption peak.

The absorption spectra of dyes anchored on a nanocrystalline TiO_2 film is displayed in Figure 4. Though the absorption tailing for the dyes in dichloromethane solution is quite similar, it moved toward high energy for **7b** in the photoanode. Generally, the dyes form aggregates at the surface of the TiO_2. A red-shift is witnessed when *J* aggregates are predominant and the dye–TiO_2 interactions are weak.[26] On the contrary, the formation of *H* aggregates at the TiO_2 surface or stronger dye–TiO_2 interactions cause a blue-shift in the absorption profile.[27] The noticeable blue-shift for the dye **7b** may be ascribed to the stronger dye–TiO_2 interactions, as the fluorene units present

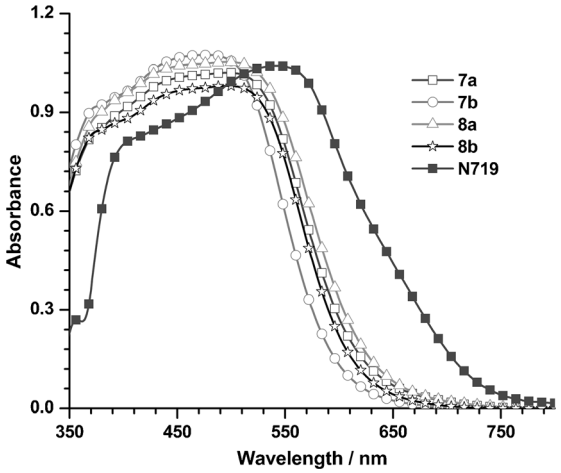

Figure 4. Absorption spectra of the dyes anchored on TiO_2.

on the donor part of the dye will inhibit the close intermolecular association of dyes at the surface of TiO_2 better than the *n*-butoxy chains. Despite the presence of the fluorene unit, elongation of conjugation due to the bithiophene segment in the linker component increases the aggregation propensity of **8b**. It is known in the literature that red-shifted absorptions of oligothiophene derivatives are due to aggregation.[5i]

The emission spectra of the dyes recorded in dichloromethane solutions (see the Supporting Information) are similar in nature and the effect of the peripheral unit is not significant. This suggests that the excited state is ICT in nature. The emission was completely quenched in polar solvents such as THF and acetonitrile (ACN) owing to the strong dipole–dipole interactions which helped the molecules non-radiatively relax into the ground state.[28]

Electrochemical Properties

The redox properties of the dyes and the precursors were examined using cyclic voltammetry. All the dyes exhibited one-electron quasireversible oxidation couple, more positive than the internal ferrocene standard (Figure 5), which originates from the removal of an electron from the triarylamine donor unit. The introduction of a *n*-butoxy or fluorene unit on the triarylamine segment increases the electron-donating strength and leads to facile oxidation compared with the parent dyes **C1** and **C2**. The order of oxidation of dyes in each series is, **7a** < **7b** and **8a** < **8b** for monothiophene and bithiophene containing dyes, respectively. Similarly the oxidation potentials of the dyes containing bithiophene (**8**) in the conjugation were low compared with the corresponding dyes with a monothiophene unit (**7**).

From the oxidation potential and the optical band gap the ground- and excited-state oxidation potentials with reference to a normal hydrogen electrode (NHE) have been deduced to appraise the electron injection and dye regeneration prospects. The energy level diagram of the dyes along with the conduction band of TiO_2 and redox potential of the electrolyte (I^-/I_3^-) is displayed in Figure 6. The ground state oxidation po-

© 2015 Wiley-VCH Verlag GmbH & Co. KGaA, Weinheim

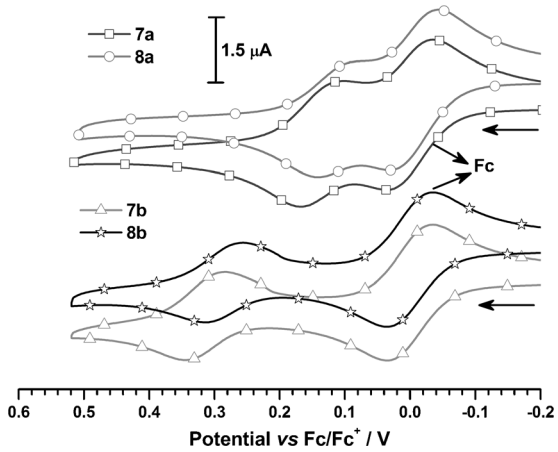

Figure 5. Cyclic voltammograms recorded for the dyes in CH_2Cl_2. Traces for **7a** and **8a** are shifted vertically for clarity.

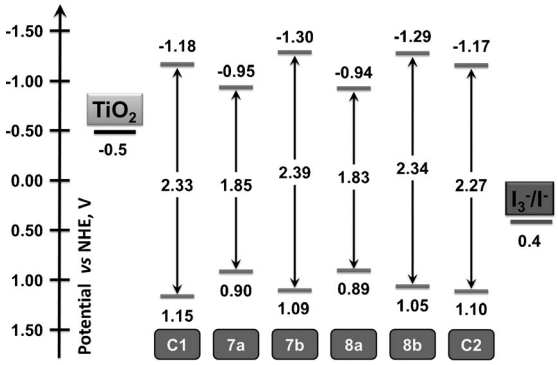

Figure 6. Energy level diagram of the materials used in the DSSCs.

tentials of the dyes range from 0.89–1.09 V vs NHE and are more positive than the redox potential of the electrolyte (0.4 vs NHE).[29] The relatively low-lying ground states of the dyes ensure a downhill electron transfer from the electrolyte to the oxidized dye to regenerate the neutral form. Similarly, the excited state potential of the dyes (−0.94–−1.30 V vs NHE) were more negative than the conduction band (CB) edge of TiO_2 (−0.5 V vs NHE).[29] The excited-state oxidation potentials of the dyes are energetically favorable for the injection of the photogenerated electrons into the conduction band of TiO_2.

The ground state potential of the dyes smaller than the parent dyes **C1** (1.15 V vs NHE) and **C2** (1.10 V vs NHE) respectively.[22] The upward shift in the ground state is more drastic for the *n*-butoxy derivatives **7a** and **8a**. However, the LUMOs of the fluorene dyes lie above the LUMO of the parent dyes **C1** (−1.18 V vs NHE) and **C2** (−1.17 V vs NHE), while those of the *n*-butoxy derivatives are destabilized. From these comparisons, it is possible to deduce that the regeneration for the new dyes is slightly less favored compared with the parent dyes. But the high-lying LUMO of the new dyes ensure a comparatively more facile electron injection into the conduction band of TiO_2. On this basis, the new dyes are expected to function as efficient sensitizers in DSSCs that produce very high photocurrent with a slight compromise in the open circuit voltage.

Theoretical Interpretations

To gain more insight into the geometry and nature of electronic transitions of the dyes we have performed the DFT calculations on the dyes. The ground state geometry of the dyes was optimized at the B3LYP/6-31G** level with tight SCF convergence.[30] The optimized geometries of the dyes were then used in the calculation of excitation energies using the MPW1 K[31] model due to the more reliable results for the donor–acceptor compounds from this model. The electronic distribution for the frontier molecular orbitals of the dyes are shown in Figure 7. The HOMOs of the dyes are mainly located on the triarylamine segment composed of diphenylamine and carbazole units and slightly diffused into the peripheral and

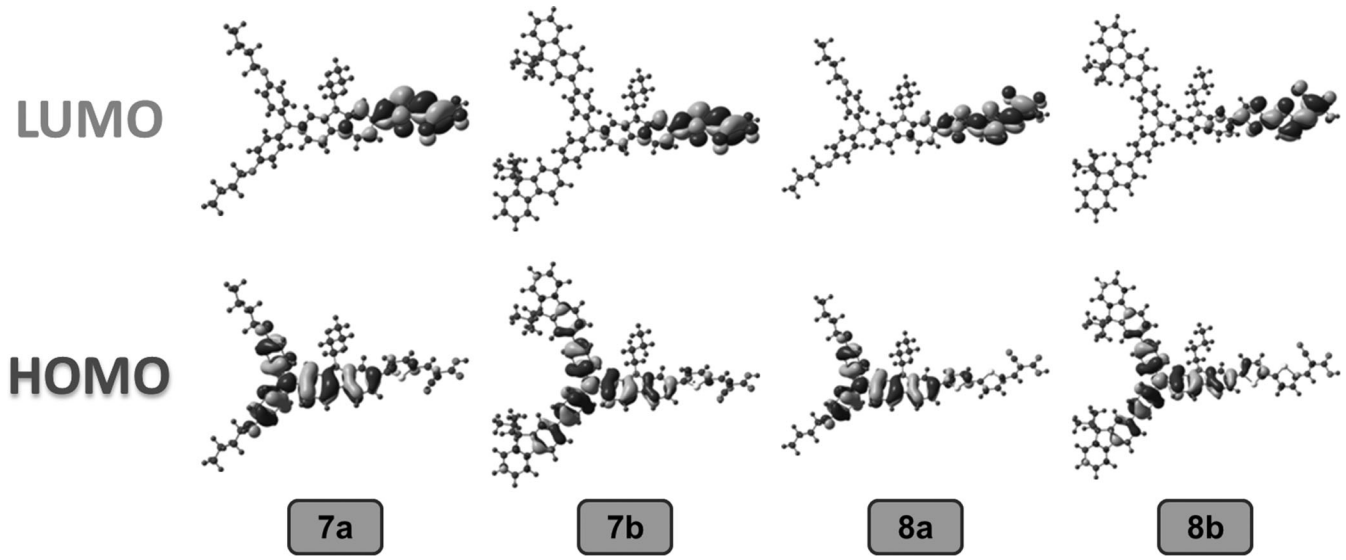

Figure 7. Electronic distribution in the frontier molecular orbitals of the dyes.

© 2015 Wiley-VCH Verlag GmbH & Co. KGaA, Weinheim

thiophene units. The main contributions to the LUMOs of the dyes are from the cyanoacrylic acid acceptor and the thiophene units. The dyes containing a bithiophene unit in the conjugation pathway have well-separated HOMOs and LUMOs, which is beneficial for charge migration from the donor to the acceptor on photoexcitation by light absorption that corresponds to the HOMO–LUMO electronic transition. Also, a slight blue-shifted ICT transition is predicted by TDDFT calculations for the fluorene derivatives. The trends in the absorption parameters in solution matched well with the computationally predicted values.

DSSC Characteristics

The photovoltaic properties of the dyes were evaluated by using them as sensitizers in Grätzel photoelectrochemical cells.[4a] The solar cells were fabricated with an effective area of 0.25 cm^2 and the electrolyte composed of LiI(0.1 M)/1,2-dimethyl-3-propylimidazolium iodide (DMPII, 0.6 M)/I_2 (0.05 M)/*tert*-butyl pyridine (TBP, 0.5 M) in an ACN, *tert*-BuOH, and DMSO mixture (3.5:3.5:3 *v/v*). The photovoltaic parameters, obtained under AM 1.5 G simulated solar light with a light intensity of 100 mW cm^{-2}, are listed in Table 2. The current-voltage characteristics and IPCE action spectra of the devices are displayed in Figure 8.

Table 2. Photovoltaic performance parameters of the DSSCs fabricated using the dyes

Dye	η [%]	V_{OC} [mV]	J_{SC} [mA cm^{-2}]	*ff*	R_{ct2} [Ω]	τ_e [ms]	R_{rec} [Ω]
C1	5.16	654	12.40	0.64	36.47	3.12	36.47
C2	5.84	644	14.50	0.63	22.94	3.12	22.94
7a	1.36	520	4.47	0.58	81.18	1.12	16.50
7b	5.76	634	14.60	0.62	20.50	8.41	23.53
8a	1.78	536	6.02	0.53	48.24	0.95	17.65
8b	4.20	596	11.50	0.61	23.53	4.63	22.35

In general, the IPCE of the devices based on the dyes containing fluorene units (**7b** and **8b**) was better than the dyes containing *n*-butoxy units (**7a** and **8a**). The lower conversion efficiencies of the *n*-butoxy derivatives may be attributed to the low molar extinction coefficients and the poor alignment of energy levels with the conduction band of TiO_2, which leads to inefficient electron injection. Between the fluorene dyes, the J_{SC} and V_{OC} values for the dye containing thiophene in the conjugation, **7b**, were higher than the bithiophene dye **8b**. Since the excited-state potentials of the dyes **7b** and **8b** are similar, the difference could not arise due to the difference in the electron injection efficiency. However, the dye **8b** has a slightly negative ground-state oxidation potential, which leads to relatively slow dye regeneration. Also, the pronounced aggregation of **8b** could also affect the light harvesting prospects. Probably, both of these characteristics contributed to the poor performance of **8b** in the DSSC. The overall conversion efficiency (η) of the device based on the dye **7b** was 5.76% with

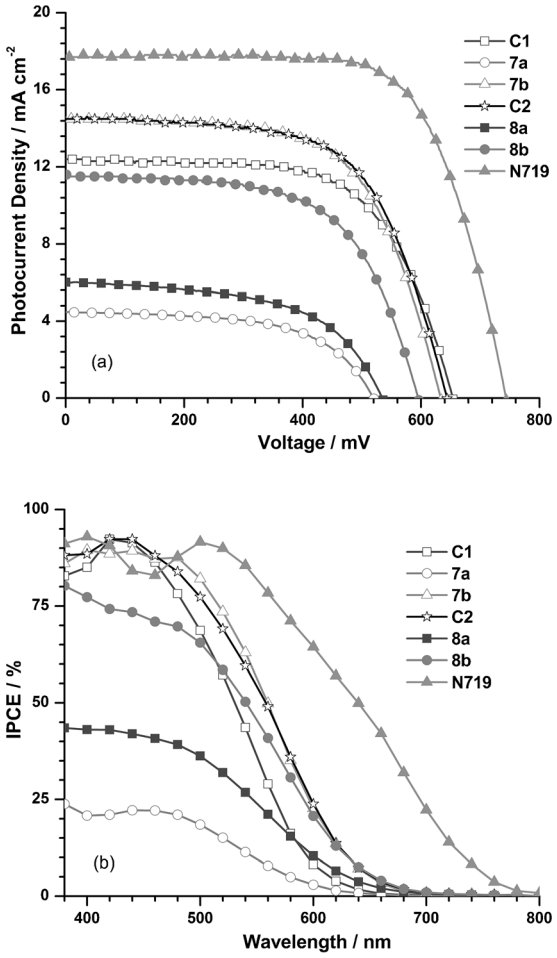

Figure 8. (a) *J-V* Characteristics and (b) IPCE plots for the DSSCs fabricated using the dyes.

a J_{SC} of 14.60 mA cm^{-2}, V_{OC} of 634 mV, and fill factor (*ff*) of 0.62. In fact, the J_{SC}, V_{OC} and *ff* values were highest for **7b**.

Electrochemical Impedance Spectroscopy

The electronic coupling of the dyes with TiO_2 and injection of excited electrons from the dye changes the electron density and causes a shift in the Fermi level of TiO_2.[4b] The shift in Fermi level alters the V_{OC} and the overall efficiency of the device. In order to scrutinize the effect of structural changes on the electron transport at the interface of the devices, we performed electrochemical impedance spectroscopy (EIS) under dark and illumination conditions.

The Nyquist plots measured for the devices under dark and illumination conditions are displayed in Figure 9. Under dark conditions, the Nyquist plots (Figure 9a) for the devices showed three semicircles. The large semicircle corresponds to the electron recombination resistance at the TiO_2/electrolyte interface and the radius of this semicircle is **7a** < **8a** < **8b** < **7b**. The larger the radius, the greater the recombination resistance (R_{rec}) for the corresponding processes, which leads to high V_{OC} values for the device.[32] On this basis it can be concluded that the fluorene-containing dyes resist electron recombination

© 2015 Wiley-VCH Verlag GmbH & Co. KGaA, Weinheim

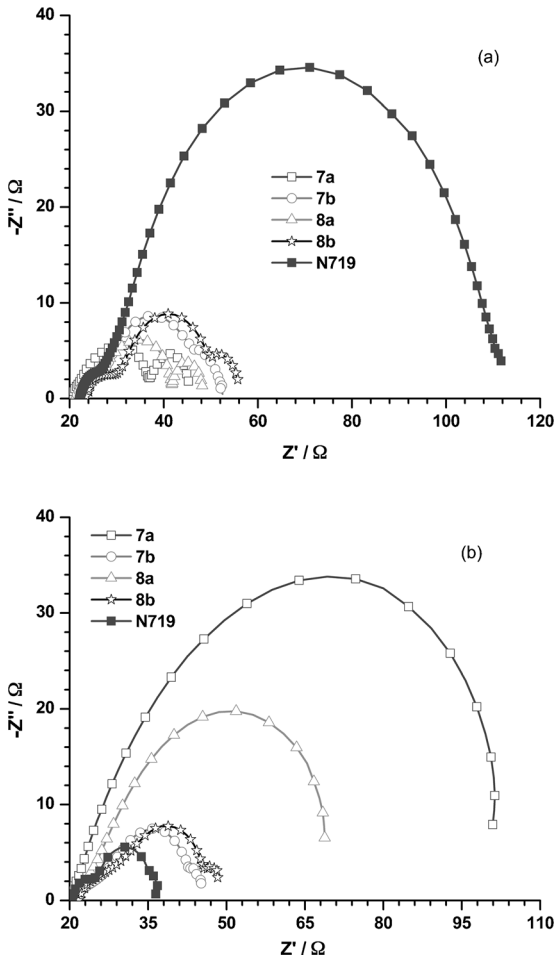

Figure 9. Nyquist plots of the DSSCs measured (a) in the dark and (b) under illumination.

better than the *n*-butoxy dyes. The enhanced electron recombination resistance for **7b** and **8b** may be attributed to the presence of the fluorene units, which keeps the iodide further away from the TiO_2. The slightly higher electron recombination rate for **8b** originates from the additional electron loss pathways due to aggregation. Therefore, the high V_{OC} for the devices comprising the fluorene dyes is attributed to the reduced back electron transfer. Similarly, the charge-transfer resistance (R_{ct}) at the TiO_2/dye/electrolyte interface was deduced from the Nyquist plots measured under illumination conditions (Figure 9b). The order of R_{ct} for the devices is **7b** < **8b** < **8a** < **7a**. The R_{ct} of the dyes **7b** and **8b** with fluorene was low, which indicates the presence of good electronic coupling between the dye and TiO_2, and this is chiefly attributed to the high-lying LUMO. Due to this the J_{SC} values for the devices based on these dyes were higher. The J_{SC} values for the devices were consistent with the R_{ct} order.

The lifetime was extracted from the mid-frequency peak of the Bode Phase plot (Figure 10) by using the formula $\tau = 1/\omega$, where $\omega = 1/2\pi f_{max}$. The electron lifetime of the devices increases in the order **8a** < **7a** < **8b** < **7b**. The highest electron lifetime for **7b** indicates the effective suppression of electron association with the electrolyte as confirmed earlier from the

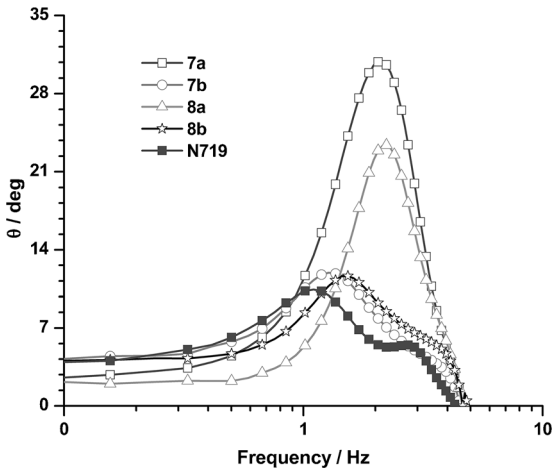

Figure 10. Bode phase plots of the DSSCs measured under illumination.

Nyquist plots.[8b] There is a clear correlation between the interfacial kinetic parameters and the device performance parameters as shown in Figure 11. The trends in the device parameters are in keeping with the charge transfer resistance and electron recombination resistance parameters. The chosen structural chromophores nicely modulated the interfacial kinetics and contributed to the good light-harvesting properties.

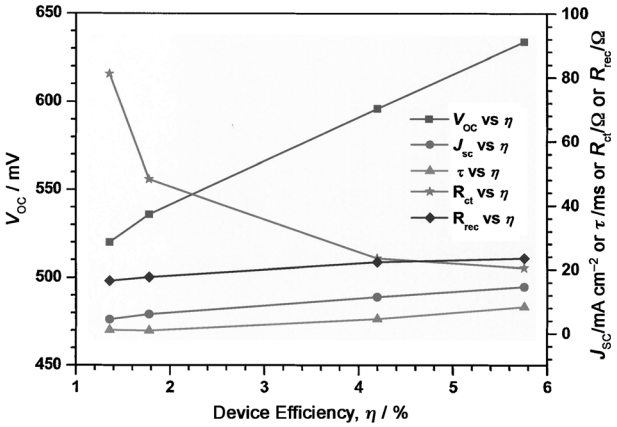

Figure 11. Correlation between the interfacial kinetic parameters and device performance parameters of the DSSCs fabricated using the dyes **C1**–**C2**, **7a**, **7b**, **8a**, and **8b**.

Conclusions

In summary, we have synthesized dyes containing different fragments in the periphery of the donor segment. These groups play distinctive roles in altering the HOMO and LUMO energies of the dyes. They provide pathways to fine-tune the electronic properties, which directly affects the electron injection and dye regeneration kinetics. Compared with the parent dyes **C1** and **C2**, the absorption of dyes containing additional chromophores on the donor units was red-shifted due to the enhanced electron richness. The incorporation of peripheral *n*-

© 2015 Wiley-VCH Verlag GmbH & Co. KGaA, Weinheim

butoxy groups significantly raised the HOMO and lowered the LUMO of the dyes relative to the parent dyes **C1** and **C2**. However, the introduction of a 9,9-diethyl-9*H*-fluorenyl group raised the LUMO compared with the parent dyes, while retaining the HOMO levels. The high-lying LUMO of the dyes **7b** and **8**b containing a 9,9-diethyl-9*H*-fluorenyl unit is favorable for abetting the electron injection into the conduction band of TiO_2 and led to the best incident photon to current conversion values. The dye **7b** achieved higher efficiency of 5.76% with promising J_{SC} of 14.60 mA cm^{-2} over the analogous parent dye **C1**. But the efficiency of dye **8b** was lower than the comparable skeleton dye **C2** owing to the relatively high-lying HOMO and enhanced aggregation propensity. Our studies illustrate that fluorene units can be effectively used to suppress electron recombination and favor electron injection.

Experimental Section

Materials and General Methods

All the precursor compounds required for the work were purchased from commercial sources and used without further purification. However, the solvents were purified and dried by standard procedures prior to use. Column chromatography purifications were performed with silica gel (230–400 mesh) as a stationary phase in a column 40 cm long and 3.0 cm in diameter. The IR spectra were recorded with a spectrophotometer using KBr pellets. The ^{1}H and ^{13}C NMR spectra were recorded with a Bruker Avance 3 NMR spectrometer operating at 500.13 and 125.77 MHz respectively. Deuterated chloroform ($CDCl_3$) and dimethyl sulfoxide ([D_6]DMSO) were used as the solvents for the measurements and the calibration was performed using the residual peak of the deuterated solvents (δ = 7.26 and 2.52 for ^{1}H; 77.0 and 39.5 for ^{13}C). UV/vis spectra were recorded at room temperature in quartz cuvettes using a Cary 100 UV/vis spectrophotometer in the range 250–1100 nm. Emission spectra were recorded using a Shimadzu RF-5301PC spectrofluorimeter at room temperature for the air equilibrated solutions. Cyclic voltammetry (CV) and differential pulse voltammetry (DPV) were performed on an BAS epsilon electrochemical workstation using a three electrode assembly comprising a glassy carbon working electrode, a non-aqueous $Ag/AgNO_3$ reference electrode, and an auxiliary platinum electrode. The experiments were performed at room temperature under a nitrogen atmosphere in dichloromethane using tetrabutylammonium perchlorate (Bu_4NClO_4, 0.1 M) as the supporting electrolyte. High-resolution mass spectra of the compounds were obtained from a Bruker Daltonik GmbH micrOTOF-QII ESI mass spectrometer in positive ion mode.

Synthesis of the Dyes

The precursors 9,9-diethyl-9*H*-fluoren-2-ylboronic acid,[33] bis(4-bromophenyl)amine[34] (**1**) and 2,7-dibromo-9-butyl-9*H*-carbazole[35] (**3**) were prepared according to literature procedures.

Bis(4-butoxyphenyl)amine (2)

In a two neck round-bottom (RB) flask a mixture of sodium (1.70 g, 73.9 mmol) was dissolved in anhydrous 1-butanol (20 mL) and bis(4-bromophenyl)amine (**1**, 1.21 g, 3.69 mmol), copper-(I)-iodide (2.96 g, 15.5 mmol), and anhydrous DMF (40 mL) were added and heated to reflux for 6 h. After the reaction, ethyl acetate (160 mL) was added, the mixture was filtered over a celite bed and washed with brine (3×75 mL). Removal of volatiles by rotary evaporation produced a solid residue. The crude product was purified by column chromatography on silica gel by using a hexanes/dichloromethane mixture (3:1) as the eluent. White solid; yield 1.94 g (62%); m.p. 78–80 °C; ^{1}H NMR ([D_6]DMSO, 500.13 MHz): δ = 7.52 (s, 1H), 6.90 (d, J = 9.0 Hz, 4H), 6.80 (d, J = 9.0 Hz, 4H), 3.90 (t, J = 6.5 Hz, 4H), 1.65–1.69 (m, 4H), 1.41–1.46 (m, 4H), 0.93 ppm (t, J = 7.5 Hz, 6H); ^{13}C NMR ([D_6]DMSO, 125.77 MHz): δ = 157.4, 143.1, 123.2, 120.4, 72.6, 36.1, 24.01, 23.9, 18.9 ppm; HRMS: *m/z*: calcd for $C_{17}H_{17}BrNO$ [*M*+H]$^+$: 314.2114; found: 314.2099.

Bis(4-(9,9-diethyl-9H-fluoren-2-yl)phenyl)amine, (2b)

A two neck RB flask charged with a mixture of **1** (1.30 g, 4 mmol), 9,9-diethyl-9*H*-fluoren-2-ylboronic acid (0.87 g, 8.8 mmol), anhydrous potassium carbonate (K_2CO_3, 3.86 g, 28 mmol) and tetrakis(-triphenylphosphine)palladium ($Pd(PPh_3)_4$, 0.27 g, 0.24 mmol) were dissolved in mixture of THF/H_2O (3:1). The reaction mixture was degassed with N_2 and refluxed for 12 h under a nitrogen atmosphere. After cooling to room temperature, the organic layer was extracted with dichloromethane and dried with sodium sulfate. The crude product was purified by column chromatography on silica gel by using a hexanes/dichloromethane mixture (2:1) as the eluent. Pale yellow solid; yield 1.31 g (54%); m.p. 184–186 °C; ^{1}H NMR ([D_6]DMSO, 500.13 MHz): δ = 8.55 (s, 1H), 7.86 (d, J = 8.0 Hz, 2H), 7.83 (d, J = 7.0 Hz, 2H), 7.70–7.72 (m, 2H), 7.64 (d, J = 8.0 Hz, 2H), 7.44 (d, J = 7.0 Hz, 2H), 7.33–7.38 (m, 4H), 7.25 (d, J = 8.5 Hz, 4H), 2.02–2.16 (m, 8H), 0.28 ppm (t, J = 7.0 Hz, 12H); ^{13}C NMR ([D_6]DMSO, 125.77 MHz): δ = 150.1, 149.5, 142.5, 140.7, 139.4, 139.0, 131.7, 127.5, 127.0, 126.9, 124.7, 122.8, 120.2, 120.1, 119.7, 117.1, 55.7, 31.8, 8.5 ppm; HRMS: *m/z*: calcd for $C_{46}H_{44}N$ [*M*+H]$^+$: 609.3390; found: 609.3363.

7-Bromo-N,N-bis(4-butoxyphenyl)-9-butyl-9H-carbazol-2-amine, (4a)

A mixture of **1** (1.96 g, 6 mmol), **2a** (0.94 g, 3 mmol), [$Pd(dba)_2$] (dba = (1*E*,4*E*)-1,5-diphenylpenta-1,4-dien-3-one; 0.02 g, 0.02 mmol), 1,2-bis(diphenylphosphino)ferrocene (dppf, 0.02 g, 0.02 mmol), sodium *tert*-butoxide (0.72 g, 7.5 mmol), and toluene was placed in a pressure tube and heated to 80 °C for 48 h. After completion of the reaction, the volatiles were removed under vacuum, and the resulting solution was extracted with dichloromethane (3×50 mL). The combined organic extracts were washed with brine solution, dried over Na_2SO_4, and concentrated. The crude product was purified by column chromatography on silica gel by using a hexanes/dichloromethane mixture (5:1) as the eluent. White solid; yield 1.30 g (71%); m.p. 60–62 °C; ^{1}H NMR ([D_6]DMSO, 500.13 MHz): δ = 7.92 (d, J = 8.0 Hz, 2H), 7.74 (d, J = 1.0 Hz, 1H), 7.26 (dd, J = 13.5 Hz, 1.5 Hz, 1H), 7.01 (d, J = 9.0 Hz, 4H), 6.88–6.90 (m, 5H), 6.72 (dd, J = 8.5 Hz, 1.5 Hz, 1H), 4.14 (t, J = 7.0 Hz, 2H), 3.94 (t, J = 6.5 Hz, 4H), 1.65–1.71 (m, 4H), 1.54–1.60 (m, 2H), 1.40–1.47 (m, 4H), 1.12–1.19 (m, 2H), 0.94 (t, J = 7.5 Hz, 6H), 0.78 ppm (t, J = 8.0 Hz, 3H); ^{13}C NMR ($CDCl_3$, 125.77 MHz): δ = 155.2, 147.9, 141.8, 141.5, 141.3, 126.2, 122.1, 121.8, 120.5, 120.4, 117.7, 116.3, 115.1, 114.8, 111.3, 101.4, 67.9, 42.6, 31.4, 30.9, 20.4, 19.3, 13.9, 13.8 ppm; HRMS: *m/z*: calcd for $C_{36}H_{41}BrN_2O_2$ [*M*]$^+$: 612.2345; found: 612.2321.

7-Bromo-9-butyl-N,N-bis(4-(9,9-diethyl-9H-fluoren-2-yl)phenyl)-9H-carbazol-2-amine, (4b)

4b was obtained from **1** (1.52 g, 4 mmol) and **2b** (1.22 g, 2 mmol) by following the procedure described above for **4a**. White solid;

© 2015 Wiley-VCH Verlag GmbH & Co. KGaA, Weinheim

yield 1.14 g (63%); m.p. 138 °C; ^{1}H NMR ($CDCl_3$, 500.13 MHz): δ = 7.94 (d, J = 8.5 Hz, 1H), 7.87 (d, J = 8.0 Hz, 1H), 7.76 (d, J = 7.5 Hz, 2H), 7.72–7.73 (m, 2H), 7.61 (d, J = 8.5 Hz, 5H), 7.58 (d, J = 1.5 Hz, 1H), 7.56 (s, 2H), 7.50 (d, J = 1.5 Hz, 1H), 7.28–7.36 (m, 11H), 7.20 (s, 1H), 7.09 (m, 1H), 4.14 (t, J = 7.0 Hz, 2H), 2.05–2.10 (m, 8H), 1.77 (t, J = 7.5 Hz, 2H), 1.32–1.34 (m, 2H), 0.91 (t, J = 7.0 Hz, 3H), 0.36–0.38 ppm (t, J = 7.5 Hz, 12H); ^{13}C NMR ($CDCl_3$, 125.77 MHz): δ = 150.6, 150.1, 147.2, 141.8, 141.2, 140.5, 139.5, 135.8, 127.8, 127.0, 125.5, 124.2, 122.9, 122.2, 121.0, 120.0, 119.7, 118.5, 117.6, 111.7, 105.2, 56.2, 43.0, 32.9, 31.0, 20.5, 13.9, 8.6 ppm; HRMS: m/z: calcd for $C_{17}H_{17}BrNO$ $[M+H]^+$: 330.0488; found: 330.0487.

5-(7-(Bis(4-butoxyphenyl)amino)-9-butyl-9H-carbazol-2-yl)thiophene-2-carbaldehyde, (5a)

A mixture of **4a** (0.61 g, 1 mmol), (5-(1,3-dioxolan-2-yl)thiophen-2-yl)tributylstannane (0.49 g, 1.1 mmol) and anhydrous DMF (5 mL) was maintained under a nitrogen atmosphere and bis(triphenylphosphine)dichloropalladium(II) ($[Pd(PPh_3)_2Cl_2]$; 0.01 g, 0.01 mmol) was added to it. The resulting reaction mixture was heated to 80 °C for 15 h. After completion of the reaction, the reaction mixture was poured into cold water and extracted with dichloromethane (3×40 mL). Removal of volatiles from the dichloromethane extract by rotary evaporation produced a solid residue. The residue was dissolved in glacial acetic acid (4 mL) and heated to 60 °C for 1 h to form a clear solution. After the addition of water (3 mL), the reaction mixture was maintained at 60 °C for an additional 1 h. Finally, the mixture was cooled and extracted with dichloromethane (3×40 mL). The dichloromethane extract was washed thoroughly with brine solution and dried over anhydrous sodium sulfate. The solid residue obtained on evaporation of the dichloromethane extract was purified by column chromatography on silica gel by using a hexanes/dichloromethane mixture (1:1) as the eluent. Yellow solid; yield 0.46 g (71%); m.p. 104 °C; IR (KBr): $\tilde{\nu}$ = 1662 cm^{-1} ($\nu_{C=O}$); ^{1}H NMR ($CDCl_3$, 500.13 MHz): δ = 9.88 (s, 1H), 7.94 (d, J = 8.0 Hz, 1H), 7.82 (d, J = 8.5 Hz, 1H), 7.74 (d, J = 4.0 Hz, 1H), 7.57 (s, 1H), 7.49–7.51 (m, 1H), 7.46–7.47 (d, J = 4.0 Hz, 1H), 7.11 (d, J = 8.5 Hz, 4H), 6.91 (d, J = 1.5 Hz, 1H), 6.84–6.89 (m, 5H), 4.13 (t, J = 7.0 Hz, 2H), 3.97 (t, J = 6.5 Hz, 4H), 1.73–1.82 (m, 6H), 1.49–1.56 (m, 4H), 1.30–1.36 (m, 2H), 1.00 (t, J = 2.5 Hz, 6H), 0.90 ppm (t, J = 7.0 Hz, 3H); ^{13}C NMR ($CDCl_3$, 125.77 MHz): δ = 182.5, 156.2, 155.2, 148.3, 142.6, 141.5, 141.1, 140.8, 137.5, 128.8, 126.3, 124.3, 123.4, 120.7, 119.7, 117.5, 116.1, 115.1, 114.5, 106.0, 100.8, 67.8, 42.4, 31.3, 30.9, 20.3, 19.1, 13.73, 13.70 ppm; HRMS: m/z: calcd for $C_{41}H_{44}N_2O_3S$ $[M]^+$: 644.3067; found: 644.3067.

5-(7-(Bis(4-(9,9-diethyl-9H-fluoren-2-yl)phenyl)amino)-9-butyl-9H-carbazol-2-yl)thiophene-2-carbaldehyde, (5b)

5b was synthesized from **4b** (0.46 g, 0.5 mmol) and ((5-(1,3-dioxolan-2-yl)thiophen-2-yl)tributylstannane (0.24 g, 0.55 mmol) by following the procedure described above for **5a**. Yellow solid; yield 0.32 g (67%); m.p. 160 °C; IR (KBr): $\tilde{\nu}$ = 1669 cm^{-1} ($\nu_{C=O}$); ^{1}H NMR ($CDCl_3$, 500.13 MHz): δ = 9.91 (s, 1H), 8.04 (d, J = 8.0 Hz, 1H), 7.98 (d, J = 8.5 Hz, 1H), 7.73–7.79 (m, 5H), 7.56–7.69 (m, 10H), 7.51 (d, J = 3.5 Hz, 1H), 7.30–7.44 (m, 10H), 7.23–7.26 (m, 1H), 7.11 (d, J = 8.5 Hz, 1H), 4.23 (t, J = 6.5 Hz, 2H), 1.79–1.85 (m, 8H), 1.79–1.85 (m, 2H), 1.34–1.39 (m, 2H), 0.86–0.95 (m, 3H), 0.37–0.40 ppm (t, J = 7.0 Hz, 12H); ^{13}C NMR ($CDCl_3$, 125.77 MHz): δ = 182.8, 156.1, 150.6, 150.1, 147.1, 146.8, 142.6, 141.9, 141.23, 141.15, 140.6, 139.4, 137.7, 136.0, 129.7, 129.2, 127.9, 127.0, 126.9, 125.5, 124.4, 124.2, 123.8, 122.9, 121.3, 121.0, 120.4, 120.0, 119.7, 118.3, 117.9, 117.5, 106.5, 104.9, 56.2, 42.8, 32.9, 31.2, 20.5, 13.9, 8.6 ppm; HRMS: m/z: calcd for $C_{67}H_{61}N_2OS$ $[M+H]^+$: 330.0488; found: 330.0487.

5-(5-(7-(Bis(4-butoxyphenyl)amino)-9-butyl-9H-carbazol-2-yl)thiophen-2-yl)thiophene-2-carbaldehyde, (6a)

6a was obtained from **4a** (0.61 g, 1 mmol) and (5-(5-(1,3-dioxolan-2-yl)thiophen-2-yl)thiophen-2-yl)tributylstannane (0.58 g, 1.1 mmol) by following the procedure described above for **5a**. Red solid; yield 0.48 g (63%); m.p. 142–144 °C; IR (KBr): $\tilde{\nu}$ = 1660 cm^{-1} ($\nu_{C=O}$); ^{1}H NMR ($CDCl_3$, 500.13 MHz): δ = 9.85 (s, 1H), 7.91 (d, J = 8.0 Hz, 1H), 7.82 (d, J = 8.5 Hz, 1H), 7.65 (d, J = 2.5 Hz, 1H), 7.50 (s, 1H), 7.43 (d, J = 8.0 Hz, 1H), 7.34 (d, J = 10.0 Hz, 2H), 7.11 (d, J = 8.5 Hz, 5H), 6.92 (s, 1H), 6.83–6.88 (m, 5H), 4.13 (t, J = 6.0 Hz, 2H), 3.96 (t, J = 6.0 Hz, 4H), 1.79 (t, J = 7.5 Hz, 6H), 1.50–1.54 (m, 4H), 1.27–1.34 (m, 2H), 1.00 (t, J = 2.5 Hz, 6H), 0.90 ppm (t, J = 7.0 Hz, 3H); ^{13}C NMR ($CDCl_3$, 125.77 MHz): δ = 182.4, 155.3, 148.1, 148.0, 147.5, 142.6, 141.4, 141.3, 141.1, 137.5, 134.3, 129.6, 127.3, 126.3, 123.74, 123.70, 123.5, 120.7, 119.8, 117.3, 116.6, 115.2, 114.7, 105.5, 101.2, 68.0, 42.5, 31.5, 31.1, 20.5, 19.3, 13.9 ppm; HRMS: m/z: calcd for $C_{45}H_{46}N_2O_3S_2$ $[M]^+$: 726.2944; found: 726.2942.

5′-(7-(Bis(4-(9,9-diethyl-9H-fluoren-2-yl)phenyl)amino)-9-butyl-9H-carbazol-2-yl)-[2,2′-bithiophene]-5-carbaldehyde, (6b)

6b was obtained from **4b** (0.46 g, 0.5 mmol) and (5-(5-(1,3-dioxolan-2-yl)thiophen-2-yl)thiophen-2-yl)tributylstannane (0.30 g, 0.55 mmol) by following the procedure described above for **5a**. Yellow solid; yield 0.31 g (61%); m.p. 178 °C; IR (KBr): $\tilde{\nu}$ = 1661 cm^{-1} ($\nu_{C=O}$); ^{1}H NMR ($CDCl_3$, 500.13 MHz): δ = 9.88 (s, 1H), 8.01 (d, J = 8.0 Hz, 1H), 7.97 (d, J = 8.5 Hz, 1H), 7.75 (d, J = 8.0 Hz, 2H), 7.72–7.73 (m, 2H), 7.67 (d, J = 9.0 Hz, 1H), 7.60–7.63 (m, 5H), 7.56–7.59 (m, 4H), 7.49 (dd, J = 8.0 Hz, 1.5 Hz, 1H), 7.37–7.40 (m, 2H), 7.34–7.37 (m, 4H), 7.32 (d, J = 1.5 Hz, 1H), 7.29–7.30 (m, 6H), 7.22 (d, J = 1.5 Hz, 1H), 7.09–7.11 (m, 1H), 4.23 (t, J = 7.0 Hz, 2H), 2.04–2.10 (m, 8H), 1.79–1.85 (m, 2H), 1.33–1.40 (m, 2H), 0.93 (t, J = 7.5 Hz, 3H), 0.38 ppm (t, J = 7.5 Hz, 12H); ^{13}C NMR ($CDCl_3$, 125.77 MHz): δ = 182.6, 150.8, 150.3, 147.9, 147.6, 147.3, 146.5, 142.6, 141.5, 141.41, 141.37, 140.7, 139.6, 137.7, 136.0, 134.7, 130.4, 128.0, 127.4, 127.14, 127.05, 125.7, 124.4, 124.1, 124.0, 123.3, 123.1, 121.3, 121.1, 120.5, 120.1, 119.8, 118.7, 117.7, 117.6, 105.9, 105.2, 56.3, 42.9, 33.0, 31.3, 20.7, 14.1, 8.8 ppm; HRMS: m/z: calcd for $C_{71}H_{62}N_2OS_2$ $[M]^+$: 1022.4298; found: 1022.4278.

(E)-3-(5-(7-(Bis(4-butoxyphenyl)amino)-9-butyl-9H-carbazol-2-yl)thiophen-2-yl)-2-cyanoacrylic acid, (7a)

The aldehyde **5a** (0.21 g, 0.33 mmol), 2-cyanoacetic acid (0.04 g, 0.5 mmol), ammonium acetate (0.04 g, 0.25 mmol), and acetic acid (5 mL) were mixed and refluxed for 24 h. The resulting red precipitate was filtered and washed several times with water and dried. The product was crystallized from a dichloromethane/hexanes mixture to obtain an analytically pure sample. Red solid; yield 0.22 g (93%); m.p. 135–137 °C; IR: $\tilde{\nu}$ = 2221 cm^{-1} ($\nu_{C\equiv N}$); ^{1}H NMR ($CDCl_3$, 500.13 MHz): δ = 8.33 (s, 1H), 7.88 (s, 1H), 7.78–7.82 (m, 2H), 7.44–7.53 (m, 3H), 7.09 (d, J = 8.5 Hz, 4H), 6.82–6.91 (m, 6H), 4.12 (t, J = 6.0 Hz, 2H), 3.95 (t, J = 8.5 Hz, 4H), 1.73–1.80 (m, 6H), 1.47–1.52 (m, 4H), 1.25–1.29 (m, 2H), 0.99 (t, J = 7.0 Hz, 6H), 0.88 ppm (t, J = 5.0 Hz, 3H); ^{13}C NMR ($[D_6]DMSO$, 125.77 MHz): δ = 164.2, 155.5, 155.3, 154.9, 148.5, 146.4, 142.7, 141.4, 141.0, 140.7, 134.4, 128.7, 126.9, 126.6, 125.0, 124.2, 121.6, 120.4, 118.7, 117.9, 117.4, 115.9, 115.7, 113.8, 106.5, 67.7, 42.0, 31.2, 30.8, 20.1, 19.2, 14.1, 13.9 ppm; HRMS: m/z: calcd for $C_{44}H_{46}N_3O_4S$ $[M+H]^+$: 734.3022; found: 734.3016.

© 2015 Wiley-VCH Verlag GmbH & Co. KGaA, Weinheim

(E)-3-(5-(5-(7-(Bis(4-butoxyphenyl)amino)-9-butyl-9H-carbazol-2-yl)thiophen-2-yl)thiophen-2-yl)-2-cyanoacrylic acid, (8a)

8a was prepared from **6a** (0.24 g, 0.33 mmol) and 2-cyano acetic acid (0.04 g, 0.5 mmol) by following the procedure described above for **7a**. Black solid; yield 0.11 g (92%); m.p. 200–202 °C; IR (KBr): $\tilde{\nu}$ = 2213 cm^{-1} ($\nu_{C\equiv N}$); ^{1}H NMR ($CDCl_3$, 500.13 MHz): δ = 8.31 (s, 1H), 7.94 (d, J = 8.0 Hz, 1H), 7.81 (d, J = 8.0 Hz, 1H), 7.68 (d, J = 4.5 Hz, 1H), 7.61 (d, J = 4.0 Hz, 1H), 7.49 (s, 1H), 7.42–7.44 (m, 2H), 7.36 (d, J = 4.0 Hz, 1H), 7.30 (s, 1H), 7.27–7.28 (m, 2H), 7.09 (d, J = 8.5 Hz, 4H), 6.83 (d, J = 8.5 Hz, 4H), 4.14 (t, J = 6.0 Hz, 2H), 3.95 (t, J = 6.5 Hz, 4H), 1.74–1.80 (m, 6H), 1.5–1.54 (m, 4H), 1.31–1.34 (m, 2H), 1.04 (t, J = 7.5 Hz, 6H), 0.89 ppm (t, J = 7.5 Hz, 3H); ^{13}C NMR ([D_6]DMSO, 125.77 MHz): δ = 164.1, 155.4, 148.1, 147.4, 145.8, 142.5, 141.3, 141.1, 140.9, 134.3, 133.8, 129.4, 128.6, 126.8, 125.3, 125.0, 123.2, 121.4, 120.3, 117.4, 116.2, 115.8, 113.9, 105.9, 67.8, 42.0, 31.2, 30.9, 20.1, 19.2, 14.1, 14.0 ppm; HRMS: *m/z*: calcd for $C_{48}H_{47}N_3O_4S_2Na$ $[M+H]^+$: 816.2900; found: 816.2877.

(E)-3-(5-(7-(Bis(4-(9,9-diethyl-9H-fluoren-2-yl)phenyl)amino)-9-butyl-9H-carbazol-2-yl)thiophen-2-yl)-2-cyanoacrylic acid, (7b)

7b was prepared from **5b** (0.34 g, 0.33 mmol) and 2-cyano acetic acid (0.04 g, 0.5 mmol) by following the procedure described above for **7a**. Red solid; yield 0.32 g (95%); m.p. 220 °C; IR (KBr): $\tilde{\nu}$ = 2215 cm^{-1} ($\nu_{C\equiv N}$); ^{1}H NMR ($CDCl_3$, 500.13 MHz): δ = 8.27 (s, 1H), 7.99 (d, J = 8.0 Hz, 1H), 7.92 (d, J = 8.5 Hz, 1H), 7.77 (s, 1H), 7.64 (d, J = 6.5 Hz, 3H), 7.60 (d, J = 3.0 Hz, 2H), 7.53 (s, 2H), 7.47–7.50 (m, 2H), 7.41 (d, J = 4.0 Hz, 2H), 7.28–7.34 (m, 10H), 7.21 (s, 2H), 7.13 (d, J = 8.5 Hz, 3H), 7.06 (d, J = 8.0 Hz, 1H), 4.14 (t, J = 6.5 Hz, 2H), 1.94–2.01 (m, 8H), 1.73–1.79 (m, 2H), 1.29–1.34 (m, 2H), 0.86 (t, J = 7.0 Hz, 3H), 0.37 ppm (t, J = 7.0 Hz, 12H); ^{13}C NMR ([D_6]DMSO, 125.77 MHz): δ = 164.2, 155.0, 150.6, 150.0, 147.0, 146.5, 142.6, 141.8, 141.28, 141.25, 141.0, 140.4, 138.9, 135.3, 134.5, 129.5, 128.1, 128.0, 127.58, 127.56, 127.48, 127.37, 125.5, 125.4, 124.5, 124.4, 123.9, 123.3, 121.1, 121.0, 120.8, 120.72, 120.68, 120.6, 120.2, 118.2, 117.1, 117.1, 117.0, 105.2, 56.1, 42.2, 32.3, 31.0, 20.2, 14.0, 8.9 ppm; HRMS: *m/z*: calcd for $C_{70}H_{62}N_3O_2S$ $[M+H]^+$: 1008.4563; found: 1008.4587.

(E)-3-(5′-(7-(Bis(4-(9,9-diethyl-9H-fluoren-2-yl)phenyl)amino)-9-butyl-9H-carbazol-2-yl)-[2,2′-bithiophen]-5-yl)-2-cyanoacrylic acid, (8b)

It was prepared from **6b** (0.34 g, 0.33 mmol) and 2-cyano acetic acid (0.04 g, 0.5 mmol) by following a procedure described above for **7a**. Red solid; yield 0.33 g (91%); m.p. 239 °C; IR (KBr): $\tilde{\nu}$ = 2213 cm^{-1}; ^{1}H NMR ([D_6]DMSO, 500.13 MHz): δ = 8.50 (s, 1H), 8.25 (d, J = 8.0 Hz, 1H), 8.13 (t, J = 7.5 Hz, 2H), 8.00 (s, 1H), 7.87 (d, J = 8.0 Hz, 2H), 7.23 (d, J = 6.5 Hz, 2H), 7.70–7.78 (m, 4H), 7.65 (d, J = 8.0 Hz, 3H), 7.57 (d, J = 8.0 Hz, 1H), 7.44 (d, J = 7.0 Hz, 2H), 7.33–7.38 (m, 4H), 7.31 (s, 1H), 7.23 (d, J = 10.0 Hz, 4H), 6.99 (d, J = 8.5 Hz, 1H), 4.36 (t, J = 7.5 Hz, 2H), 2.04–2.14 (m, 8H), 1.68–1.71 (t, J = 7.0 Hz, 2H), 1.25 (t, J = 6.0 Hz, 2H), 0.84 (t, J = 4.0 Hz, 3H), 0.27 ppm (t, J = 7.5 Hz, 12H); ^{13}C NMR ([D_6]DMSO, 125.77 MHz): δ = 164.1, 150.6, 150.0, 147.3, 147.1, 146.2, 146.1, 142.4, 141.8, 141.4, 141.0, 140.4, 138.9, 135.8, 135.1, 134.1, 130.3, 128.0, 127.6, 127.4, 125.5, 125.1, 124.4, 123.8, 123.3, 122.9, 121.8, 120.8, 120.6, 120.2, 118.5, 117.2, 105.4, 56.1, 42.3, 32.3, 31.1, 20.2, 14.0, 8.9 ppm; HRMS: *m/z*: calcd for $C_{74}H_{64}N_3O_2S_2$ $[M+H]^+$: 1089.4362; found: 1089.4373.

Computational Methods

The Gaussian 09 program package[36] was used to perform all the calculations. The ground-state geometries were fully optimized without any symmetry constraints using DFT and Becke's[37] hybrid correlation functional B3LYP[30] with 6-31g (d,p) basis set for all atoms. Vibrational analysis on the optimized structures was performed to confirm the structure. The excitation energies and oscillator strengths for the lowest 10 singlet-singlet transitions at the optimized geometry in the ground state were obtained by TD-DFT calculations using the basis set MPW1K .[31]

Device Fabrication and Characterization

The TiO_2 colloid solution was prepared from the TiO_2 precursor by the sol-gel method as described below. Titanium(IV) tetraisopropoxide (72 mL) was added to aqueous nitric acid (430 mL, 0.1 M) with constant stirring and heated to 85 °C simultaneously for 8 h. After cooling the reaction mixture to room temperature, the resultant colloid was heated in an autoclave at 240 °C for 12 h to allow the TiO_2 particles to grow uniformly (ca. 20 nm). Consequently, the TiO_2 colloidal solution was concentrated to 10 wt% (with respect to the TiO_2). The transparent layer was prepared by the addition of PEG (25 wt% with respect to the TiO_2) to the above solution to control the pore diameters to prevent the film from cracking during drying. The scattering layer was prepared from a TiO_2 paste containing 50 wt% of light scattering TiO_2 particles (PT-501A, 15 $m^2 g^{-1}$, 100 nm, 99.74%) with respect to the 20 nm synthesized TiO_2 particles for reducing light loss by back scattering.

A fluorine-doped SnO_2 conducting glass (FTO, 7 Ω sq^{-1}, transmittance ca. 80%) was first cleaned with a neutral cleaner and then washed with deionized water, acetone, and isopropyl alcohol, sequentially. The conducting surface of the FTO was treated with a solution of titanium tetraisopropoxide (1.0 g) in 2-methoxyethanol (3.0 g) to obtain a good mechanical contact between the conducting glass and TiO_2 film, as well as to isolate the conducting glass surface from the electrolyte. TiO_2 pastes were coated on the conducting glass of FTO by the doctor blade technique. For each coating of the TiO_2 layer, the dried TiO_2 film was gradually heated to 450 °C in an air flow and subsequently sintered at that temperature for 30 min. Finally, the FTO was coated with a transparent layer (thickness 14.0 μm) and scattering layer (thickness 4.5 μm) of TiO_2 . After sintering at 450 °C and cooling to 80 °C, the TiO_2 film was immersed in a dye bath (3×10^{-4} M) at room temperature for 24 h. The absorption spectrum of the dye-loaded film was measured with a JASCO V-570 UV/vis spectrophotometer. The standard ruthenium complex, **N719**,[4g] was dissolved in acetonitrile and *tert*-butyl alcohol (volume ratio of 1:1) to make a reference dye solution. Various organic dye solutions were prepared in a mixing solvent containing ACN, *tert*-butanol, and DMSO (volume ratio of 3.5:3.5:3). The hermetically sealed cell was prepared by connecting two electrodes by a hot melt 25 μm-thick surlyn film (SX1170–25) with the TiO_2/dye film as the working electrode and a platinum-sputtered conducting glass electrode (ITO, 7 Ω $sq.^{-1}$, transmittance > 80%) as the counter electrode. The electrolyte consisting of LiI (0.1 M), DMPII (0.6 M), I_2 (0.05 M), and TBP (0.5 M) in 3-methoxypropionitrile (MPN)/ACN (volume ratio of 1:1) was introduced into the cell by capillary and the hole was sealed with hot-melt glue after the injection of the electrolyte.

The irradiation source for the measurement of photocurrent-voltage was class-A quality solar simulator (XES-301S, AM1.5G) with incident intensity (100 mW cm^{-2}) and the surface of the DSSC covered by a mask with a light-illuminated area of 0.16 cm^2. The light intensity was calibrated with a standard Si Cell (PECSI01). The pho-

© 2015 Wiley-VCH Verlag GmbH & Co. KGaA, Weinheim

toelectrochemical characteristics of the DSSCs were measured with a potentiostat/galvanostat. For the electrochemical impedance spectra, a potentiostat/galvanostat (PGSTAT 30, Autolab, ECO-Chemie) equipped with an FRA2 module was used under a constant light illumination of 100 mW cm^{-2} and the range of frequency applied was 10 MHz–65 kHz. The impedance spectra were analyzed using an equivalent circuit model. Incident IPCE curves were obtained under short-circuit conditions. The light source was a class A quality solar simulator (PEC-L11, AM 1.5 G); light was focused through a monochromator onto the photovoltaic cell. The monochromator was incremented through the visible spectrum to generate the IPCE (λ) as defined by IPCE (λ) = 1240 ($J_{SC}/\lambda\phi$), where λ is the wavelength and J_{SC} is the short-circuit photocurrent (mA cm^{-2}) recorded with a potentiostat/galvanostat, and ϕ is the incident radiative flux (W m^{-2}) measured with an optical detector and power meter.

Acknowledgements

Financial support from the Department of Science and Technology, India, to K.R.J.T. and a senior research fellowship to A.V. are gratefully acknowledged. We also thank the DST for a grant to purchase an ESI mass spectrometer via the FIST program.

Keywords: carbazoles · chromophores · dye-sensitized solar cells · electrochemical impedance spectroscopy · organic dyes

[1] a) T. Leijtens, I.-K. Ding, T. Giovenzana, J. T. Bloking, M. D. McGehee, A. Sellinger, *ACS Nano* **2012**, *6*, 1455 – 1462; b) K. R. Justin Thomas, J. T. Lin, Y.-T. Tao, C.-W. Ko, *J. Am. Chem. Soc.* **2001**, *123*, 9404 – 9411; c) J. Li, D. Liu, Y. Li, C.-S. Lee, H.-L. Kwong, S. Lee, *Chem. Mater.* **2005**, *17*, 1208 – 1212; d) W.-Y. Hung, G.-C. Fang, Y.-C. Chang, T.-Y. Kuo, P.-T. Chou, S.-W. Lin, K.-T. Wong, *ACS Appl. Mater. Interfaces* **2013**, *5*, 6826 – 6831.

[2] a) A. R. Murphy, J. M. J. Fréchet, *Chem. Rev.* **2007**, *107*, 1066 – 1096; b) C. Wang, H. Dong, W. Hu, Y. Liu, D. Zhu, *Chem. Rev.* **2012**, *112*, 2208 – 2267; c) J. Zaumseil, H. Sirringhaus, *Chem. Rev.* **2007**, *107*, 1296 – 1323.

[3] a) A. W. Hains, Z. Liang, M. A. Woodhouse, B. A. Gregg, *Chem. Rev.* **2010**, *110*, 6689 – 6735; b) M. Grätzel, *Acc. Chem. Res.* **2009**, *42*, 1788 – 1798.

[4] a) B. O'Regan, M. Grätzel, *Nature* **1991**, *353*, 737 – 740; b) A. Mishra, M. K. R. Fischer, P. Bäuerle, *Angew. Chem. Int. Ed.* **2009**, *48*, 2474 – 2499; *Angew. Chem.* **2009**, *121*, 2510 – 2536; c) A. Hagfeldt, G. Boschloo, L. Sun, L. Kloo, H. Pettersson, *Chem. Rev.* **2010**, *110*, 6595 – 6663; d) J. N. Clifford, E. Martínez-Ferrero, A. Viterisi, E. Palomares, *Chem. Soc. Rev.* **2011**, *40*, 1635 – 1646; e) Y. Wu, W. Zhu, *Chem. Soc. Rev.* **2013**, *42*, 2039 – 2058; f) W. Ying, J. Yang, M. Wielopolski, T. Moehl, J.-E. Moser, P. Compte, J. Hua, S. M. Zakeeruddin, H. Tian, M. Grätzel, *Chem. Sci.* **2014**, *5*, 206 – 214; g) M. K. Nazeeruddin, A. Kay, I. Rodicio, R. Humphry-Baker, E. Müller, P. Liska, N. Vlachopoulos, M. Grätzel, *J. Am. Chem. Soc.* **1993**, *115*, 6382 – 6390.

[5] a) C. Lambert, J. Schelter, T. Fiebig, D. Mank, A. Trifonov, *J. Am. Chem. Soc.* **2005**, *127*, 10600 – 10610; b) P. Singh, A. Baheti, K. R. J. Thomas, *J. Org. Chem.* **2011**, *76*, 6134 – 6145; c) H. Choi, C. Baik, S. O. Kang, J. Ko, M.-S. Kang, M. K. Nazeeruddin, M. Grätzel, *Angew. Chem. Int. Ed.* **2008**, *47*, 327 – 330; *Angew. Chem.* **2008**, *120*, 333 – 336; d) A. Venkateswararao, P. Tyagi, K. R. J. Thomas, P.-W. Chen, K.-C. Ho, *Tetrahedron* **2014**, *70*, 6318 – 6327; e) M. Velusamy, K. R. J. Thomas, J. T. Lin, Y.-C. Hsu, K.-C. Ho, *Org. Lett.* **2005**, *7*, 1899 – 1902; f) J. M. Raimundo, P. Blanchard, N. Gallego-Planas, N. Mercier, I. Ledoux-Rak, R. Hierle, J. Roncali, *J. Org. Chem.* **2002**, *67*, 205 – 218; g) P. Tyagi, A. Venkateswararao, K. R. J. Thomas, *J. Org. Chem.* **2011**, *76*, 4571 – 4581; h) J. Seo, S. Kim, S. Y. Park, *J. Am. Chem. Soc.* **2004**, *126*, 11154 – 11155; i) A. Venkateswararao, K. R. J. Thomas, C.-P. Lee, C.-T. Li, K.-C. Ho, *ACS Appl. Mater. Interfaces* **2014**, *6*, 2528 – 2539; j) K. R. J. Thomas, N. Kapoor, C.-P. Lee, K.-C. Ho, *Chem. Asian J.* **2012**, *7*, 738 – 750.

[6] a) Z. Ning, H. Tian, *Chem. Commun.* **2009**, 5483 – 5495; b) M. Liangw, J. Chen, *Chem. Soc. Rev.* **2013**, *42*, 3453 – 3488; c) S. Cai, X. Hu, Z. Zhang, J. Su, X. Li, A. Islam, L. Han, H. Tian, *J. Mater. Chem. A* **2013**, *1*, 4763 – 4772; d) S. Cai, G. Tian, X. Li, J. Su, H. Tian, *J. Mater. Chem. A* **2013**, *1*, 11295 – 11305.

[7] a) Z. Ning, Q. Zhang, W. Wu, H. Pei, B. Liu, H. Tian, *J. Org. Chem.* **2008**, *73*, 3791 – 3797; b) J. Tang, J. Hua, W. Wu, J. Li, Z. Jin, Y. Long, H. Tian, *Energy Environ. Sci.* **2010**, *3*, 1736 – 1745; c) Z. Wan, C. Jia, Y. Duan, L. Zhou, J. Zhang, Y. Lin, Y. Shi, *RSC Adv.* **2012**, *2*, 4507 – 4514; d) M.-D. Zhang, H. Pan, X.-H. Ju, Y.-J. Ji, L. Qin, H.-G. Zheng, X.-F. Zhou, *Phys. Chem. Chem. Phys.* **2012**, *14*, 2809 – 2815.

[8] a) Z. Wang, M. Liang, L. Wang, Y. Hao, C. Wang, Z. Sun, S. Xue, *Chem. Commun.* **2013**, *49*, 5748 – 5750; b) A. Yella, R. Humphry-Baker, B. F. E. Curchod, N. A. Astani, J. Teuscher, L. E. Polander, S. Mathew, J.-E. Moser, I. Tavernelli, U. Rothlisberger, M. Grätzel, M. K. Nazeeruddin, J. Frey, *Chem. Mater.* **2013**, *25*, 2733 – 2739; c) L. E. Polander, A. Yella, J. Teuscher, R. Humphry-Baker, B. F. E. Curchod, N. A. Astani, P. Gao, J.-E. Moser, I. Tavernelli, U. Rothlisberger, M. Grätzel, M. K. Nazeeruddin, J. Frey, *Chem. Mater.* **2013**, *25*, 2642 – 2648; d) Z. Wang, M. Liang, Y. Hao, Y. Zhang, L. Wang, Z. Sun, S. Xue, *J. Mater. Chem. A* **2013**, *1*, 11809 – 11819.

[9] a) E. Gabrielsson, H. Ellis, S. Feldt, H. Tian, G. Boschloo, A. Hagfeldt, L. Sun, *Adv. Energy Mater.* **2013**, *3*, 1647 – 1656; b) D.-Y. Chen, Y.-Y. Hsu, H.-C. Hsu, B.-S. Chen, Y.-T. Lee, H. Fu, M.-W. Chung, S.-H. Liu, H.-C. Chen, Y. Chi, P.-T. Chou, *Chem. Commun.* **2010**, *46*, 5256 – 5258; c) M. Zhang, Y. Wang, M. Xu, W. Ma, R. Li, P. Wang, *Energy Environ. Sci.* **2013**, *6*, 2944 – 2949.

[10] A. Baheti, K. R. J. Thomas, C.-P. Lee, C.-T. Li, K.-C. Ho, *J. Mater. Chem. A* **2014**, *2*, 5766 – 5779.

[11] D. P. Hagberg, X. Jiang, E. Gabrielsson, M. Linder, T. Marinado, T. Brinck, A. Hagfeldt, L. Sun, *J. Mater. Chem.* **2009**, *19*, 7232 – 7238.

[12] a) T. Khanasa, N. Jantasing, S. Morada, N. Leesakul, R. Tarsang, S. Namuangruk, T. Kaewin, S. Jungsuttiwong, T. Sudyoadsuk, V. Promarak, *Eur. J. Org. Chem.* **2013**, 2608 – 2620; b) S. Namuangruk, R. Fukuda, M. Ehara, J. Meeprasert, T. Khanasa, S. Morada, T. Kaewin, S. Jungsuttiwong, T. Sudyoadsuk, V. Promarak, *J. Phys. Chem. C* **2012**, *116*, 25653 – 25663; c) T. Sudyoadsuk, S. Pansay, S. Morada, R. Rattanawan, S. Namuangruk, T. Kaewin, S. Jungsuttiwong, V. Promarak, *Eur. J. Org. Chem.* **2013**, 5051 – 5063.

[13] M. Cheng, X. Yang, F. Zhang, J. Zhao, L. Sun, *J. Phys. Chem. C* **2013**, *117*, 9076 – 9083.

[14] L. Zhou, C. Jia, Z. Wan, X. Chen, X. Yao, *Org. Electron.* **2013**, *14*, 1755 – 1762.

[15] a) S. Kim, J. K. Lee, S. O. Kang, J. Ko, J.-H. Yum, S. Fantacci, F. D. Angelis, D. D. Censo, M. K. Nazeeruddin, M. Grätzel, *J. Am. Chem. Soc.* **2006**, *128*, 16701 – 16707; b) B. Liu, Q. Liu, D. You, X. Li, Y. Naruta, W. Zhu, *J. Mater. Chem.* **2012**, *22*, 13348 – 13356; c) B. Liu, B. Wang, R. Wang, L. Gao, S. Huo, Q. Liu, X. Li, W. Zhu, *J. Mater. Chem. A* **2014**, *2*, 804 – 812.

[16] J. F. Hartwig, *Angew. Chem. Int. Ed.* **1998**, *37*, 2046 – 2067; *Angew. Chem.* **1998**, *110*, 2154 – 2177.

[17] N. Miyaura, A. Suzuki, *Chem. Rev.* **1995**, *95*, 2457 – 2483.

[18] J. K. Stille, *Angew. Chem. Int. Ed. Engl.* **1986**, *25*, 508 – 524; *Angew. Chem.* **1986**, *98*, 504 – 519.

[19] G. Evano, N. Blanchard, M. Toumi, *Chem. Rev.* **2008**, *108*, 3054 – 3131.

[20] M. Holzapfel, C. Lambert, *J. Phys. Chem. C* **2008**, *112*, 1227 – 1243.

[21] E. Knoevenagel, *Chem. Ber.* **1896**, *29*, 172 – 174.

[22] A. Venkateswararao, K. R. J. Thomas, C.-P. Lee, K.-C. Ho, *Tetrahedron Lett.* **2013**, *54*, 3985 – 3989.

[23] a) O. van den Berg, W. F. Jager, S. J. Picken, *J. Org. Chem.* **2006**, *71*, 2666 – 2676; b) A. Granzhan, H. Ihmels, G. Viola, *J. Am. Chem. Soc.* **2007**, *129*, 1254 – 1267.

[24] A. Baheti, P. Tyagi, K. R. J. Thomas, Y.-C. Hsu, J. T. Lin, *J. Phys. Chem. Lett.* **2009**, *113*, 8541 – 8547.

[25] a) M. K. Nazeeruddin, et al., *J. Am. Chem. Soc.* **2001**, *123*, 1613 – 1624; for complete reference, see the Supporting Information; b) M. K. Nazeeruddin, S. M. Zakeeruddin, R. Humphry-Baker, M. Jirousek, P. Liska, N. Vlachopoulos, V. Shklover, C. H. Fisher, M. Grätzel, *Inorg. Chem.* **1999**, *38*, 6298 – 6305.

[26] K. Sayama, S. Tsukagoshi, K. Hara, Y. Ohga, A. Shinpou, Y. Abe, S. Suga, H. Arakawa, *J. Phys. Chem. B* **2002**, *106*, 1363 – 1371.

[27] C. Teng, X. Yang, C. Yang, H. Tian, S. Li, X. Wang, A. Hagfeldt, L. Sun, *J. Phys. Chem. C* **2010**, *114*, 11305 – 11313.

© 2015 Wiley-VCH Verlag GmbH & Co. KGaA, Weinheim

[28] a) R. Potyrailo, K. Rajan, K. Stoewe, I. Takeuchi, B. Chisholm, H. Lam, *ACS Comb. Sci.* **2011**, *13*, 579 – 633; b) K. Rurack, J. L. Bricks, G. Reck, R. Radeglia, U. Resch-Genger, *J. Phys. Chem. A* **2000**, *104*, 3087 – 3109; c) J. A. Pollard, D. Zhang, J. A. Downing, F. J. Knorr, J. L. McHale, *J. Phys. Chem. A* **2005**, *109*, 11443 – 11452.
[29] a) M. Grätzel, *Nature* **2001**, *414*, 338 – 344; b) A. Hagfeldt, M. Grätzel, *Chem. Rev.* **1995**, *95*, 49 – 68.
[30] R. G. Parr, W. Yang, *Annu. Rev. Phys. Chem.* **1995**, *46*, 701 – 728.
[31] B. J. Lynch, P. L. Fast, M. Harris, D. G. Truhlar, *J. Phys. Chem. A* **2000**, *104*, 4811 – 4815.
[32] a) S. R. Raga, E. M. Barea, F. Fabregat-Santiago, *J. Phys. Chem. Lett.* **2012**, *3*, 1629 – 1634; b) G. Li, M. Liang, H. Wang, Z. Sun, L. Wang, Z. Wang, S. Xue, *Chem. Mater.* **2013**, *25*, 1713 – 1722.
[33] Y.-S. Yen, Y.-C. Chen, Y.-C. Hsu, H.-H. Chou, J. T. Lin, D.-J. Yin, *Chem. Eur. J.* **2011**, *17*, 6781 – 6788.
[34] E. Ishow, A. Brosseau, G. Clavier, K. Nakatani, R. B. Pansu, J.-J. Vachon, P. Tauc, D. Chauvat, C. R. Mendoncüa, E. Piovesan, *J. Am. Chem. Soc.* **2007**, *129*, 8970 – 8971.
[35] a) A. W. Freeman, M. Urvoy, M. E. Criswell, *J. Org. Chem.* **2005**, *70*, 5014 – 5019; b) Y. Che, D. E. Gross, H. Huang, D. Yang, X. Yang, E. Discekici, Z. Xue, H. Zhao, J. S. Moore, L. Zang, *J. Am. Chem. Soc.* **2012**, *134*, 4978 – 4982.
[36] Gaussian 09, Revision A.02, M. J. Frisch, et al., Gaussian, Inc.: Wallingford, CT, **2009**; for complete reference, see the Supporting Information.
[37] a) A. D. Becke, *J. Chem. Phys.* **1993**, *98*, 1372 – 1377; b) C. Lee, W. Yang, R. G. Parr, *Phys. Rev. B* **1988**, *37*, 785 – 789.

Received: November 6, 2014
Published online on November 25, 2014

© 2015 Wiley-VCH Verlag GmbH & Co. KGaA, Weinheim